

**The Cosmic Background Explorer's time-ordered data is also consistent with the absence of anisotropies in the cosmic microwave background**

**Keith S Cover**  
**Keith@kscover.ca**

**Abstract**

The data measured by the Cosmic Background Explorer's (COBE) differential microwave radiometer (DMR) has been shown to be consistent with the existence of 10ppm anisotropies in the cosmic microwave background (CMB). This consistency has been widely accepted as a definitive detection of the anisotropies. However, the reanalysis presented in this paper shows that the COBE DMR data is also consistent with the absence of anisotropies. Consequently, the probability densities of the sky maps with and without anisotropies are comparable. Provided it is confirmed that the COBE data is also consistent with the non existence of the 10ppm anisotropies, it is argued that the COBE data alone tells nothing more about the existence of the anisotropies than was known before the COBE satellite was launched. As WMAP has the same differential data acquisition and reconstruction algorithm as COBE, it is quite possible that a similar reanalysis of the WMAP data will lead to the same conclusion. The single beam antenna and low noise receivers of the soon-to-be-launched Planck satellite should permit direct measurement of the 10ppm anisotropies and provide definitive evidence as to their existence or non existence.

## Introduction

Precise and accurate measurement of anisotropies in the cosmic microwave background (CMB) would provide a treasure trove of information on the cosmos. As a consequence, tremendous effort has been expended on trying to detect and measure any anisotropies. These efforts have included two satellite missions that have published results, COBE (Smoot et al. 1992; Bennett et al. 1996A) and WMAP (Bennett et al. 2003; Spergel et al. 2003), and the Planck satellite scheduled to be launched in early 2008 (Tauber 2004).

The original COBE analysis reported detecting anisotropies at roughly 10 ppm of the CMB temperature. The WMAP mission, which closely followed the COBE acquisition and reconstruction strategy but improved on the spatial resolution, reported detecting similar anisotropies. Both COBE and WMAP used a differential microwave radiometry (DMR). The DMR's, rather than measuring the intensity of the CMB at a point in the sky, measured the difference between two beams separated by 60°. A map of the fluctuations in the intensity of the CMB at each point in the sky was then reconstructed by finding a sky map that was consistent with the DMR measurements.

A major impediment to measuring the anisotropies in the CMB is the dust concentrated near the galactic plane. As the dust at the galactic centre is up to 1000 times brighter than the reported anisotropies in the CMB (Barnes et al. 2003), great care must be taken to ensure the dust signal does not contaminate the measurements away from the galactic band. While most of the dust lies within 20° of the galactic plane, at some longitudes it extends several degrees further (Kogut et al. 1996).

An inherent problem in designing any reconstruction algorithm is dealing with the nonuniqueness of the result – the fact that many different sky maps can be consistent with the same data set (Press et al. 1992). In designing their reconstruction algorithm, the original COBE reconstruction dealt with the nonuniqueness by using the maximum likelihood fit to the data. Thus, they chose the sky map that fit the data as well as possible as determined by the  $\chi^2$  measure (Press et al. 1992).

By all accounts the COBE team put tremendous time, care and effort into ensuring the reported detection was as reliable as possible (Kugut et al. 1992; Smoot 1993; Mather & Boslough 1996). However, the author can find nothing in the literature to suggest that anyone has considered the possibility that the COBE data may be also consistent with a sky map that does not have any anisotropies. While it is a common practice in image reconstruction not to explicitly consider this possibility, it leaves the analysis incomplete.

Maximum likelihood has been widely used to design image reconstruction algorithms for many years. While it has important successes it has also performed less well than expected on some problems. For example, in designing multiexponential reconstruction algorithms, its results are often disappointing (Istratov and Vyvenko, 1999). Also, while maximum likelihood is a popular way to derive the discrete Fourier transform reconstruction algorithm, as is well known, the resulting reconstruction algorithm generates sidelobes (also called Gibb's phenomena or truncation artefacts) when applied to signals with large peaks. These sidelobes, if not

taken into account by interpreters, can lead to false positive detection of signal, for example, MRI image reconstruction (Wood and Henkelman 1985; Frank et al. 1997).

To examine the possibility that the COBE DMR data is also consistent with a sky map that has no anisotropies, a reanalysis was completed using a modified maximum likelihood reconstruction algorithm that forced all pixels to zero that were beyond a specified number of degrees from the galactic plane. The specified degrees was then varied from  $90^\circ$  to  $0^\circ$  and the best fit by the  $\chi^2$  measure was calculated for each. The sky maps and  $\chi^2$  values were then examined to determine of no anisotropies was also consistent with the COBE DMR data.

The nonuniqueness of the image reconstruction problem is an unresolved issue in many fields. For example, the multiexponential reconstruction problem is much simpler to state mathematically than COBE's but is also nonunique. As a result, there is no consensus on how to reconstruct multiexponential decays. A particular problem in multiexponential reconstruction, the myelin peak detection problem, is surprisingly similar to the CMB anisotropy problem. Both are trying to detect a small signal which is adjacent to a much larger one and both problems are routinely tackled using reconstruction algorithms. Indeed, the modified maximum likelihood algorithm used in this paper was originally designed by the author for the myelin peak detection problem (Cover 2006).

This paper is not the first to raise questions about the results reported by COBE and WMAP. Concerns about the unusual characteristics of some of the results have been raised previously (Starkman and Schwarz 2005). Nevertheless, it is essential for the progress of science that the fundamental basis for assessing the reliability of any experimental results be the quality of the experimental technique and analysis rather than the consistency of the results with various theories.

## Method

The time order data (TOD) for COBE consisted of 3 pairs of channels. The frequency of each pair were 31.5, 53 and 90 GHz. Each channel pair had two polarisations labelled A and B. Channel 31B was not used in this reanalysis because of poor data quality. Bennett et al. (1996A), averaged together sky maps of the A and B channel pairs after reconstruction to improve the signal to noise ratio (SNR) and the displayed the results as a sky map for each frequency. In this analysis, the A and B channels sky maps will be presented separately to provide independent confirmation of the results.

For both the original reconstruction and this reanalysis the COBE TOD was fitted to a pixelized sky map,  $T_j$ , consisting of 6144 pixels. The fitting was accomplished for each channel using the maximum likelihood criterion. Maximum likelihood requires the minimisation of the equation

$$\chi^2 = \sum_{\tau} \left[ \frac{D_{ij}(t) - (T_i - T_j)}{\sigma_{ij}(t)} \right]^2 \quad (\text{EqChi2})$$

over the time,  $t$ , where  $D_{ij}(t)$  is the TOD,  $\sigma_{ij}(t)$  is the noise of the pixel pair,  $ij$ , observed at time  $t$  (Kogut et al. 1996). The larger the value of  $\chi^2$  the poorer the fit of the data to a potential sky map,  $T_i$ . The range of values of  $\chi^2$  for which the sky map is considered inconsistent with the data is somewhat arbitrary. Assuming ideal Gaussian

noise, the expected value for  $\chi^2$  is the number of data points,  $N$ , and the standard deviation of  $\chi^2$  is  $(2N)^{1/2}$  (Press et al. 1992). Many would consider a  $\chi^2$  value that falls within 2 standard deviations of its expected value to be a good fit to the TOD.

For convenience, the original COBE analysis used the normalised  $\chi^2$  values in place of the actual  $\chi^2$  values. The normalised  $\chi^2$  values were calculated by dividing the actual  $\chi^2$  values by  $N$ .

It is possible to calculate a probability density of a particular sky map directly from the  $\chi^2$  using the equation

$$\text{Prob}(\chi^2) = k \exp\left(-\frac{1}{2}\chi^2\right) \quad (\text{EqProb})$$

(Press et al. 1992 p 820) where  $k$  is a constant independent of  $\chi^2$ . Thus the probability density of any sky maps is completely determined by its  $\chi^2$  fit to data. An important property of the relationship between  $\chi^2$  and the probability density is that the probability density strictly decreases with increasing  $\chi^2$ . The TOD has insufficient information to calculate probabilities from probability densities. Consequently, a probability cannot be calculated without prior information (Tarantola 1987). As no reliable prior information exists the probabilities cannot be calculated.

The COBE TOD used for the reanalysis were the 4-year “pixelized” differential data files download from the Legacy Archive for Microwave Background Data Analysis (LAMBDA) web site maintained by the Goddard Space Flight Center. The data in the files included corrections for known systematic error and subtraction of a nominal dipole to minimise pixel gradient effects.

The numerical optimization was implemented using the conjugate gradient algorithm (Press et al. 1992). Pixels further than a specified number of degrees from the galactic equator were constrained to zero in a simple way. The initial values for all pixels in all optimisations were set to zero. In addition, for all pixels that were to be constrained to zero during an optimization, the corresponding gradient was forced to zero. This ensured the required pixel values would remain unchanged at zero as desired.

To double check the results of the reanalysis, the sky maps with all pixels more than  $24^\circ$  forced to zero were used to generate simulated pixelized data. The simulated data was then reconstructed using the same reconstruction algorithm as used by the original COBE analysis (maximum likelihood with all 6144 pixels free to change). The simulated data was generated in two different forms: one with instrumentation noise added and one without. All simulated data was generated from sky maps before the application of any smoothing.

In addition, 5 different version of simulated data for channel 31A were generated including instrumentation noise. The only difference between the 5 cases of simulated data was the value used to seed the random number generator used to generate the simulated noise. Again, the simulated data was reconstructed using the same reconstruction algorithm as the original COBE analysis.

Smoothing and display of the sky maps closely follows the steps described in Bennett et al. (1996B) including smoothing with a  $7^{\circ}$  Gaussian filter and the use of Mollweide projections.

All calculations were performed on a PC with a 1200MHz Athlon CPU with 512MB of memory and written in Java. The time to calculate a single sky map for a single channel was between 5 and 10 minutes.

## Results

Fig. 1 shows how the normalised  $\chi^2$  values varies with an increasing number of constrained pixels for each of the 5 reconstructed channels. The increasing number of constrained pixels from  $90^{\circ}$  to  $24^{\circ}$  shows little change in the  $\chi^2$  values but below  $24^{\circ}$  they begin to show a distinct increase.

The  $\chi^2$  values at  $0^{\circ}$  indicate how consistent the data from each channel is with a sky map with no signal. In both Fig. 1 and Table 1, all channels show a clear increase in the  $\chi^2$  values at  $0^{\circ}$  as compared to  $90^{\circ}$ . Channel 31A shows the highest increase suggesting the poorest fit to no signal and thus the highest signal from the galactic band. Channels 53A and 53B show intermediate increases and channels 90A and 90B show the lowest.

Table 1 shows the precise value of the normalised  $\chi^2$  values for the original reconstruction from the original COBE analysis as well as the values from the reanalysis at  $90^{\circ}$ ,  $24^{\circ}$  and  $0^{\circ}$ . The  $\chi^2$  values for the  $90^{\circ}$  and  $24^{\circ}$  sky maps using the modified maximum likelihood algorithm are slightly less than those of the original reconstructions by the original COBE analysis of the 4 year data (Bennett et al. 1996B) for all channels except 31A. For 31A the  $\chi^2$  value is only slightly larger. Thus, from Eq (EqProb), the probability densities of the sky maps are also very similar. These similarities between the original COBE reconstructions and the modified maximum likelihood algorithm presented in this paper confirm that the modified maximum likelihood algorithm is behaving as it should.

Fig. 2 shows the sky maps reconstructed from the 5 channels with no pixels constrained to zero. As expected, since the same reconstruction algorithm was used, these sky maps match those presented by Bennett et al. (1996A) including the  $\chi^2$  values. This match is apparent from examination of the features in the galactic band.

Fig. 3 shows the sky maps that have pixels further than  $24^{\circ}$  from the galactic equator constrained to zero. From table 1, these sky maps are also consistent with the pixelized data. In addition, as follows from equation (EqProb), the sky maps showing the nonexistence of the anisotropies have comparable probability densities to the one showing the anisotropies existence.

Fig. 4 shows the sky maps reconstructed, with no pixels constrained to zero, from the simulated data from the sky maps in Fig. 3, with added instrumentation noise. The similarities between the sky map reconstructed from the COBE data (Fig. 2) and the simulated data are striking for all channels even though the simulated data contains no anisotropies.

Fig. 5 shows reconstruction, with no pixels constrained to zero, of the simulated data without any instrumentation noise added. The most notable characteristic of sky maps is the lack of structure beyond  $24^\circ$  of the galactic equator. This is not too surprising given the sky maps used to generate the simulated data (Fig. 3) had no structure. However, the pixel values beyond  $24^\circ$  of the galactic equator are all nonzero even though the sky maps used to generate the simulated data had all pixels beyond  $24^\circ$  set to zero.

Fig. 6 shows the simulated data for channel 31A reconstructed, with no pixels constrained to zero, with different realisations of the noise. All the sky maps in this figure look similar to each other and to channel 31A in Fig 2.

## Discussion

Fig. 1 shows the normalised  $\chi^2$  values versus the latitude of the constrained pixels. The noise of the TOD is to a good approximation uncorrelated Gaussian (Kogut et al. 1992). As there are over 100,000,000 measurements for each channel, according to the probability theory presented in the methods section the normalised  $\chi^2$  values should be within 0.0001 of unity. The  $\chi^2$  values in the original COBE analysis actually varied from 1.18 to 0.93 as they do in this reanalysis. This discrepancy is discussed in Bennett et al. (1996B) and is attributed to a change in the noise of the channels from pre-flight measurement to in-flight measurements.

Even though the drift in the standard deviation of the noise is likely far less than the change during launch, it is also likely to be greater than 0.0001. Therefore, no reliable threshold can be applied to the  $\chi^2$  values to determine whether any particular sky map is, or is not, consistent with the data. Therefore, for sake of discussion, we will consider any  $\chi^2$  value as consistent if they are sufficiently "close" to that of the  $\chi^2$  value of sky maps reconstructed with no pixels constrained to zero.

In Fig. 1, the flatness of the  $\chi^2$  values from  $90^\circ$  to  $24^\circ$  for all channels strongly suggests the COBE TOD data is consistent with all pixel values beyond of  $24^\circ$  of the galactic equator being zero. In addition, the increasing values of the  $\chi^2$  from  $24^\circ$  to  $0^\circ$  also indicates there is signal in the region of the galactic band. This detection of the galactic band confirms the reanalysis is sensitive to signal and supports the results that the COBE TOD is consistent with no anisotropies outside of  $24^\circ$ .

Table 1 provides the differences between the  $\chi^2$  values at  $90^\circ$  and  $0^\circ$  for each channel. These differences monotonically decrease with frequency. This trend is consistent with the synchrotron emission from the galactic band decreasing with increase frequency, as is reported in the literature (Smoot et al. 1993).

The correspondence of the sky maps in Fig. 2 with those provided by Bennett et al. (1996A) is inline with the proper functioning of the reconstruction software.

Fig 3. displays the sky maps that have all pixels beyond  $24^\circ$  forced to zero for all channels. As mentioned in the results, all these maps are also consistent with the COBE pixelized data. This sky maps strongly support the hypothesis that the COBE TOD is also consistent with no CMB anisotropies.

The striking similarity between the sky maps in Fig. 2 and Fig. 4 demonstrates that combination of the COBE data acquisition and reconstruction algorithm, when applied to a sky with no anisotropies as in Fig. 3, can generate false positive anisotropies very similar to those reported detected by the original COBE analysis.

Fig 5's. absence of variation in pixel values beyond  $24^\circ$  of the galactic band suggests the variation in the COBE sky map beyond  $24^\circ$  could be due to instrumentation noise. This inference is because the only difference between the sky maps in Fig. 4 and Fig. 5 is the absence of the instrumentation noise in simulated data in Fig 5. The nonzero value of the pixels beyond  $24^\circ$  that is consistent with the simulated data is entirely possible because of the differential nature of the COBE data acquisition. As a consequence of the differential acquisition, if the same constant value is added to all pixels in a sky map, the sky map's  $\chi^2$  measure of consistency with the data will be unchanged.

The fact that all of Fig. 6 sky map look similar to channel 31A in Fig.2 indicates the instrumentation noise, although uncorrelated in the simulated data, is highly correlated by the reconstruction algorithm. This high correlation of the instrumentation noise in the reconstruction image makes it easier to mistake for signal.

#### WMAP

The WMAP mission design closely followed that of COBE with the major exceptions of larger antenna area and lower noise electronics. Significantly, WMAP used both the  $60^\circ$  angle between the two differential antennas and the reconstruction algorithm used by the COBE mission (Bennett et al. 2003). Thus, it would not be surprising if WMAP data would also be consistent with no anisotropies. Thus it would be worthwhile to repeat the reanalysis presented in this paper on WMAP TOD data. The outcome should be similar to that of the COBE TOD data

#### *Reported Earth based detections*

A host of groups have reported detecting of anisotropies in the CMB using ground based or airborne detectors. An extensive list of studies is included in Bennett et al. (2003). It may seem implausible to suggest that so many highly capable groups have all independently arrived at the same false positive detection of anisotropies. However, such an occurrence is not unprecedented. Matthews et al. (2004) describes a case where at least 7 different ground-based studies reported the detection of p-mode frequencies in the photometry of the star Procyon. The confidence the detection was so high that Procyon was considered one of the best candidates for asteroseismology.

Much higher quality photometric data, returned by the MOST space-based telescope, showed the reported ground-based detections to be incorrect. Matthews et al. showed a possible cause of the repeated false positive detection of the p-mode frequencies could be traced to the algorithm used to reconstruct the frequency spectrum from ground the based photometry. The reconstruction algorithm was based on the Fourier transform but was modified with the intent of handling gaps in the ground-based photometry due to the rotation of the earth. Matthews et al. showed these modifications could have inadvertently caused the false positive results. As we have

much more experience using the Fourier transform in image reconstruction than we do with the image reconstruction algorithm used for COBE, the possibility of a false positive detection of anisotropies in the CMB using ground based measurement must be given serious consideration.

### *Planck*

The Planck mission is currently scheduled for launch in early 2008. The current mission profile calls for a 30 months of operations including two complete surveys of the full sky, each requiring between 12 and 14 months of observing time (Tauber 2004). The satellite will rotate at 1 revolution per minute. As the satellite rotates, the FOV will trace a circle of  $170^\circ$  on the sky. The circle will be displaced in small increments over each day so the total average displacement per day will be about  $1^\circ$ . Thus the whole sky will be scanned in about 6 months. The sky maps will be reconstructed from the many intersecting circles of data.

The anisotropies reported by COBE should be detectable directly by Planck by averaging many repetitions of the same circle. Smoothing of the TOD could be employed to substantially reduce the number of repetitions. While the smoothing would limit the spatial extent of anisotropies that could be detected, confirming the 10 ppm anisotropies reported by COBE would only require spatial resolution of about  $10^\circ$ . Estimating the number of repetitions required to definitively confirm or rule out 10 ppm anisotropies would require detailed signal and noise analysis. But is likely safe to assume that, during the 30 month mission, enough time could be found to repetitively measure several circles.

## **Conclusions**

This paper has raised two questions. The first is whether the detection of 10ppm anisotropies in the CMB reported by COBE should be taken as a reasonably reliable detection of the anisotropies. It has been shown the COBE data is, to a good approximation, as consistent with no anisotropies as it is with their existence at 10ppm. Thus, any claims of detection based solely on the COBE TOD data are not substantiated by this reanalysis and the existence of the anisotropies cannot be established to any acceptable probability. In addition, the possibility must be considered that the signals reported as anisotropies may actually be instrumentation noise that has been highly correlated and had its mean offset by the maximum likelihood reconstruction algorithm that was used in the original COBE analysis.

The second question raised was whether the 10ppm anisotropies exist at all given other reports of their detection. While other experiments have also claimed to have detected the anisotropies, most of their measurements are confounded by the earth's atmosphere and/or used similar reconstruction algorithms to COBE's.

The Planck satellite should be able to provide a definitive answer as to the existence of 10 ppm anisotropies by direct measurement because of its single beam antenna and low noise performance. However, if the CMB anisotropies exist but are substantially less than 10 ppm, it is unclear how effective Planck will be in their detection. If circumstances permit, some sort of prelaunch modification to Planck that would allow

wider beam sizes that could be selected on orbit, in addition to the one currently planned, might be worth considering.

## References

Barnes C., et al., 2003, "First year Wilkinson microwave anisotropy probe (WMAP) observations: Galactic signal contamination from sidelobe pickup," *ApJS*, 148, 51

Bennett C.L., et al. 1996A, "4-Year COBE DMR Cosmic Microwave Background Observations: Maps and Basic Results," *ApJ*, 464, L1

ed. Bennett C.L., Leisawitz D, Jackson P.D., 1996B, "COBE-DMR Four-year project data sets (PDS), analyzed science data sets (ASDS), and galactic coordinate data sets explanatory supplements" COBE Ref Pub. No. 96-B (Greenbelt, MD; NASA/GSFC), available in electronic form from the NSSDC.

Bennett C.L., et al. 2003, "First year Wilkinson microwave anisotropy probe (WMAP) observations: preliminary maps and basic results," *ApJS*, 148, 1

Cover K.S., 2006, "A multiexponential reconstruction algorithm immune to false positive peak detection", *Rev. Sci. Instrum.*, In press (Currently available online at [rsi.aip.org](http://rsi.aip.org) in the July 2006 issue).

Frank L.R., Brossman J., Buxton R.B., Resnick D., 1997, "MR imaging truncation artifacts can create a false laminar appearance in cartilage.", *American Journal of Roentgenology*, 168, 547

Istratov A.A, Vyvenko O. F., 1999, "Exponential analysis in physical phenomena", *Rev. Sci. Instr.* 70, 1233

Kogut A. et al., 1992, "COBE differential microwave radiometers – preliminary systematic error analysis," *ApJ*, 401, 1

Kogut A., Banday A.J., Bennett C. L., Gorski K. M., Hinshaw G., Smoot G. F., Wright E. L., 1996, "Microwave emissions at high Galactic latitudes in the four-year DMR sky maps," *ApJ*, 464, L5

Mather J.C., Boslough J, 1996, *The very first light: the true inside story of the scientific journey back to the dawn of the universe*. Basic Books, New York

Matthews J.M., Kusching R., Guenther D.B., Walker G.A., Moffat A.F.J., Rucinski S.M., Sasselov D., Weiss W.W., 2004, "No stellar p-mode oscillations in spaced-based photometry of Procyon," *Nature*, 430, 51

Press W.H., Teukolsky S.A., Vetterling W.T., Flannery B.P., 1992, *Numerical recipes in C*. Cambridge Univ. Press, Cambridge

Smoot G., 1992, "Structure in the COBE differential microwave radiometer: 1<sup>st</sup> year maps," *ApJ*, 396, L1

Smoot G., 1993, Wrinkles in time: the imprint of creation. Abacus, London

Spergel D.N. et al., 2003, "First year Wilkinson microwave anisotropy probe (WMAP) observations: determination of cosmological parameters," ApJS, 148, 175

Starkman G. D. and Schwarz D. J., 2005, "Is the universe out of tune?", Scientific American, 293, 48

Tauber J. A., 2004, "The Planck mission", Advances in space research, 34, 491

Tarantola A., 1987, Inverse Problem Theory, Elsevier, Amsterdam

Wood M.L., Henkelman R.M., 1985, "Truncation artifacts in magnetic resonance imaging", Magnetic resonance in medicine, 2, 517

## Figure Captions

**Figure 1.** Graph of the  $\chi^2$  values versus the number of degrees from the galactic equator beyond which the pixels were constrained to zero. As can be seen from the plots, there was virtually no change in the  $\chi^2$  values between  $90^\circ$  and  $24^\circ$ . The horizontal axis is labelled in units of degrees but is spaced by percentage of the pixels that are not constrained to zero.

**Figure 2.** Sky maps reconstructed as part of the reanalysis with none of the 6144 pixels constrained to zero and thus matching the original COBE reconstructions. The sky maps clearly show the signal from the galactic band is many times larger than that of the apparent anisotropies.

**Figure 3.** Sky maps reconstructed as part of the reanalysis with pixel further than  $24^\circ$  from the galactic equator constrained to zero. The sky maps are, for all practical purposes, as consistent with the COBE TOD data as when no pixels are constrained to zero (Fig. 2). As all of the pixels more than  $24^\circ$  from the galactic equator are zero. Thus, the COBE data is also consistent with no CMB anisotropies.

**Figure 4.** Sky maps reconstructed from simulated data generated from the sky maps in Fig. 3. Instrumentation noise was added as part of the generation of the simulated data. The similarity between all of the 5 sky maps in this figure and the corresponding maps in Fig. 2 supports the conclusion that the COBE data is also consistent with no anisotropies.

**Figure 5.** Sky maps reconstructed from simulated data generated from the sky maps in Fig. 3 but with no instrumentation noise added. The lack of the variation in the region beyond  $24^\circ$  from the galactic equator supports the hypothesis that the variation in the pixels at more than  $24^\circ$  is due to instrumentation noise. It is proposed in the text that the offset from zero of the pixels more than  $24^\circ$  from the galactic equator is a consequence of the differential nature of the COBE measurements combined with the maximum likelihood.

**Figure 6.** The sky map for channel 31A reconstructed from 5 different cases of simulated data that differ only in the realisation of the instrumentation noise. The similarity between all of the sky maps in this figure and those of 31A in Fig. 2 support the hypothesis that the variation in the sky map pixels more than  $24^\circ$  from the galactic equator is primarily due to instrumentation noise.

## Tables

**Table 1.** The  $\chi^2$  values from the original COBE analysis (Bennett et al 1996B) compared with the reanalyses for all 6144 pixels ( $90^\circ$ ) and for pixels constrained to zero further than  $24^\circ$  degrees of the galactic plane. In all but one case the  $\chi^2$  values for  $90^\circ$  and  $24^\circ$  are below those of the original analysis indicating the reanalysis sky maps are just as consistent with the data as the original sky maps. The one exception (31A,  $b < 24^\circ$ ) is only slightly larger than the reanalysis and still can be considered consistent with the data.

Channel	Number of observations	Normalized chi2 (Bennett et al. 1996B)	Normalized chi2 ( $b < 90^\circ$ )	Normalized chi2 ( $b < 24^\circ$ )	Normalized chi2 ( $b = 0^\circ$ )	Differences in Normalized chi2's ( $b=90$ and $b = 0^\circ$ )
31A	168,132,225	1.12200079	1.12118002	1.12359839	1.15818237	0.03700235
53A	218,557,665	1.05689634	1.05410233	1.05668081	1.07795510	0.02385277
53B	218,586,649	1.18697517	1.18123414	1.18397989	1.20146171	0.02022757
90A	218,398,620	0.94087681	0.93740007	0.93941973	0.94313518	0.00573511
90B	218,360,156	1.18006973	1.17460992	1.17721477	1.18330889	0.00869897

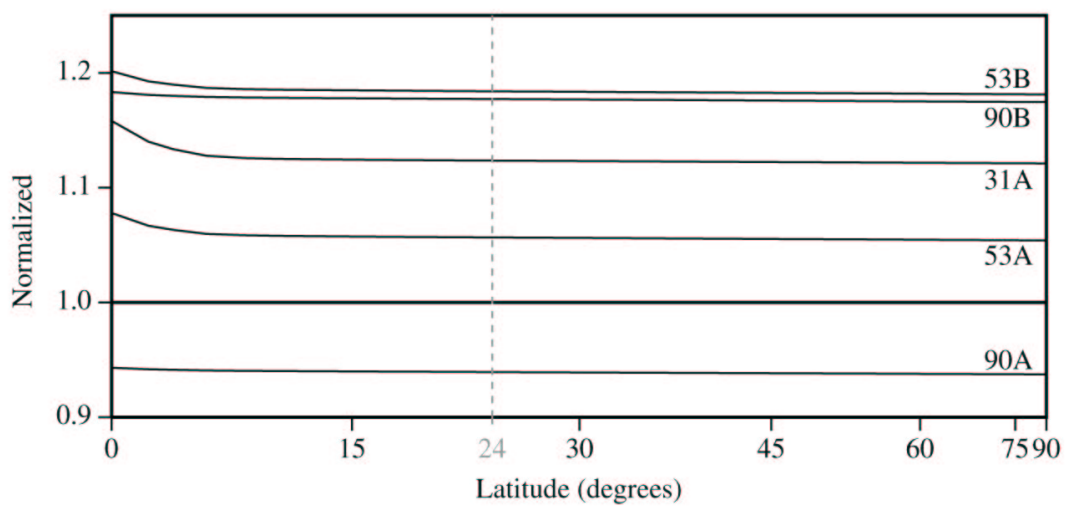


Figure 1

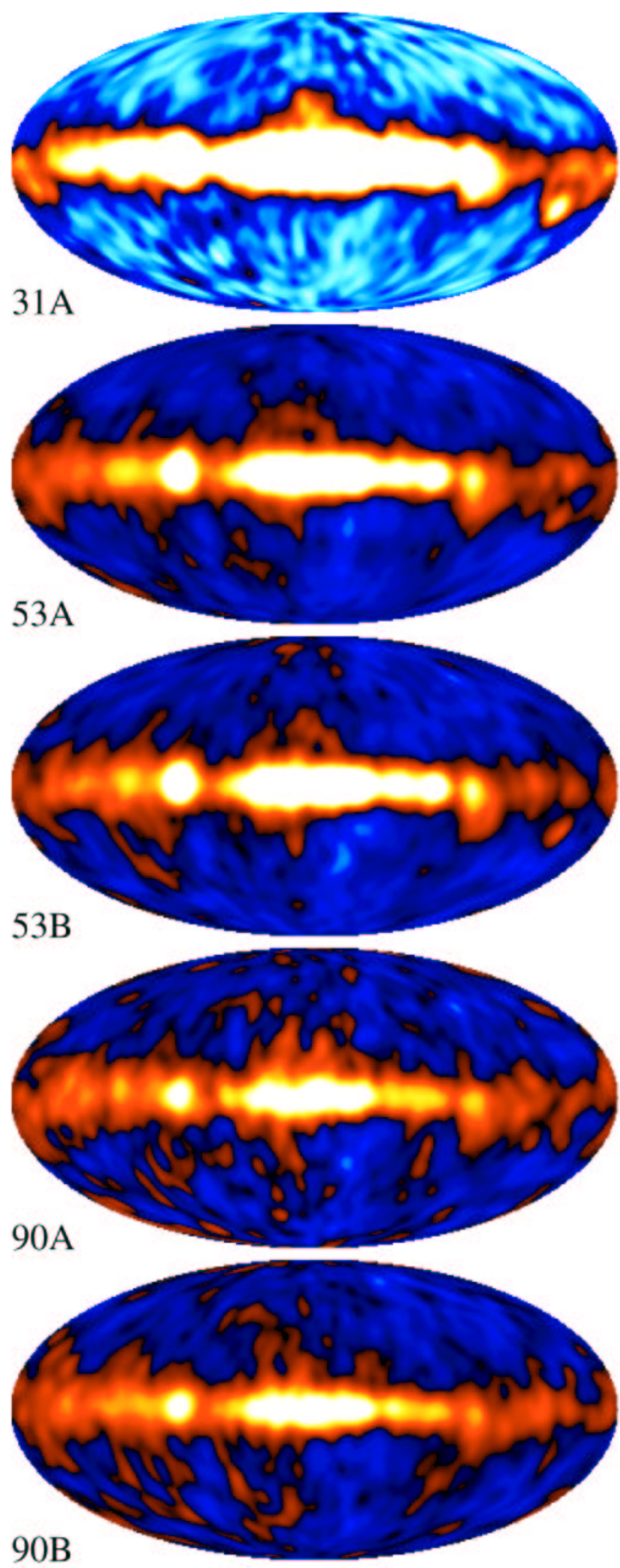


Figure 2

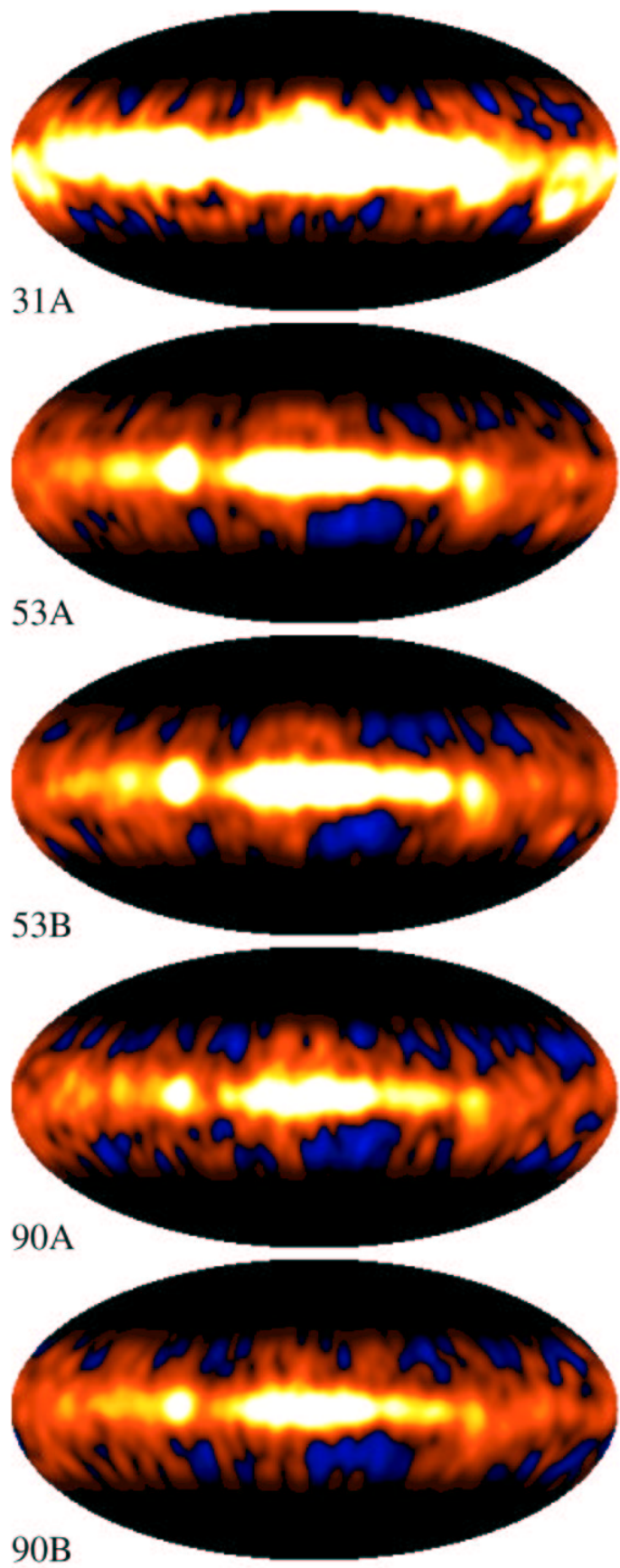


Figure 3

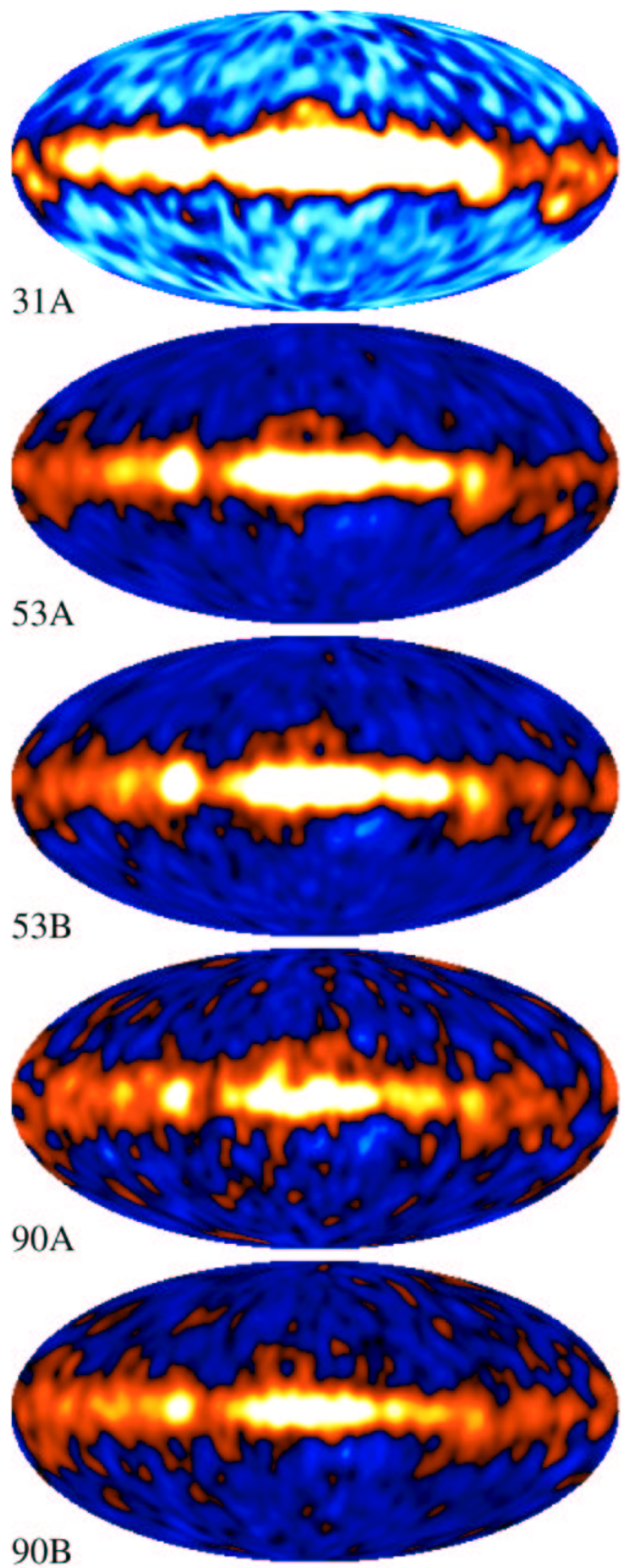


Figure 4

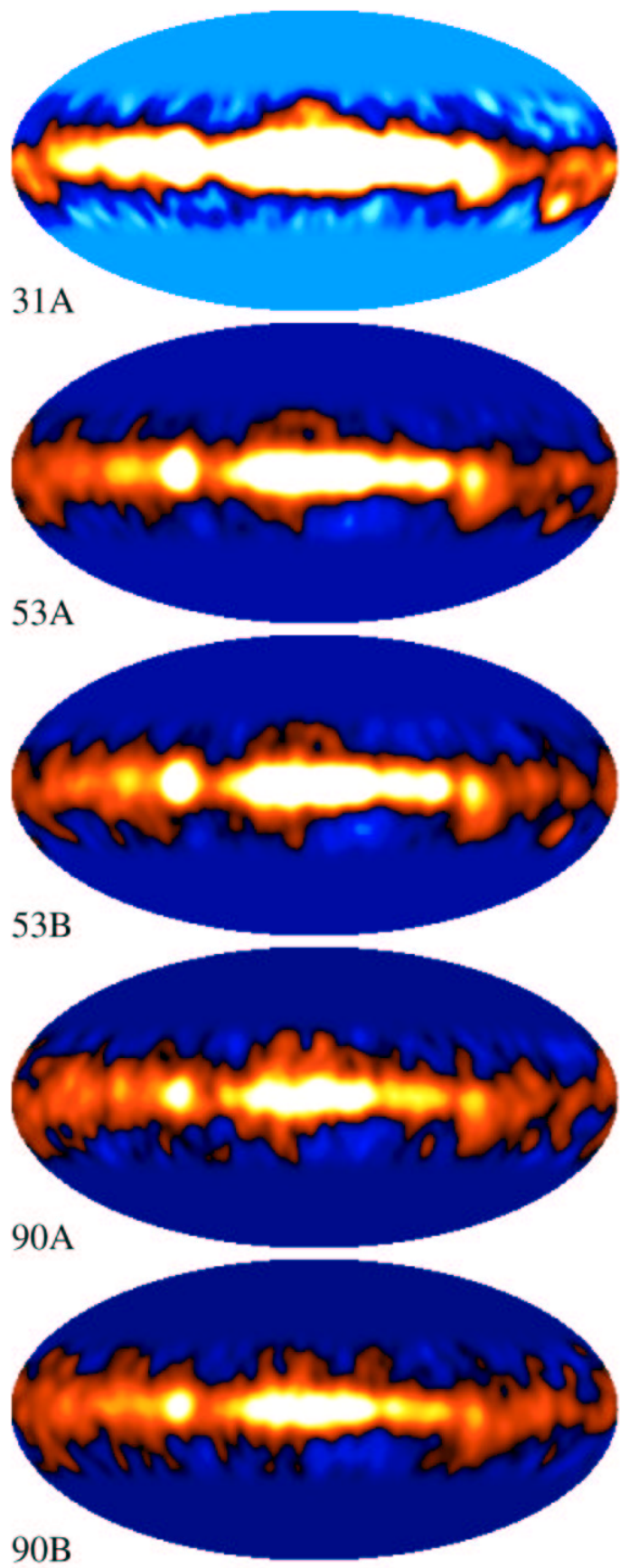


Figure 5

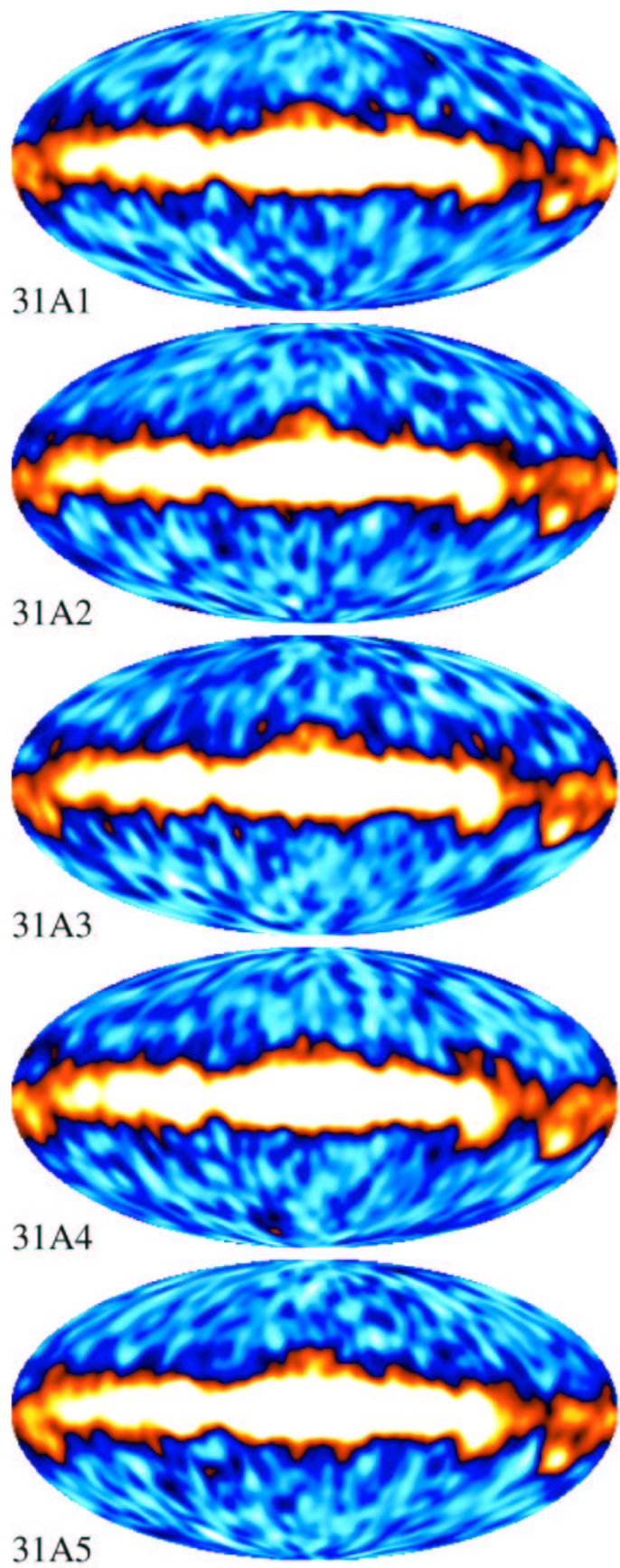


Figure 6